WIND ENERGY
Wind Energ. 0000; **00**:1–16
DOI: 10.1002/we

RESEARCH ARTICLE

Wind tunnel investigation on the effect of the turbine tower on the wake symmetry of wind turbines in single and tandem arrangement

Fabio Pierella[1], Lars Sætran [1]

[1] Norwegian University of Science and Technology, N-7043

ABSTRACT

The symmetry in the wake mean velocity of one and two three-bladed wind turbines ($D = 0.9\ m$) was investigated by means of wind tunnel experiments in the closed-loop wind tunnel of the Norwegian University of Science and Technology, Trondheim, NO. The wake of the single turbine expanded more in the horizontal than in the vertical direction, and the center of the wake vortex had a tendency to move towards the wind tunnel floor as it was advected downstream from the rotor. The wake of the turbine tandem showed a similar behaviour, with a larger degree of non-symmetry.
The analysis of the cross-stream velocity profiles revealed that the non-symmetries were caused by a different cross-stream momentum transport in the top-tip and bottom-tip region, induced by the turbine tower wake. In fact, when a second additional turbine tower, mirroring the original one, was installed above the turbine nacelle, the wake recovered its symmetric structure.

KEYWORDS

wind ; turbine ; wake ; tower ; symmetry ; tandem

Correspondence

Email: lars.saetran@ntnu.no

Received . . .

1. INTRODUCTION

The wake of a three-bladed wind turbine consists in an axisymmetric helical vortex system, which trails downstream from the turbine rotor, see e.g. [1]. Such a vortex system is conditionally stable, and its breakdown limits can be mathematically derived [2].

In practice, the vortex system and therefore the wind turbine wake are never perfectly symmetric. Some of the most important reasons for that are the interaction between the blade root and the turbine nacelle which destabilizes the root vortex, the presence of shear and background turbulence in the mean flow, the pitch differences between the individual blades, and the influence of the wind turbine tower. These disturbances lead to the breakdown of the vortex system into a turbulent wake flow with distinctive characteristics, see for example [3].

For most of these factors, the effect of on the wake structure is well known. For example, the tests in [4, 5] show how the shear, turbulence and the stratification in the mean flow affect the breakdown and the evolution of the wake vortex structure. In particular, higher shear and turbulence levels in the background flow lead to higher stress in the top-tip region of the turbine wake.

As for the effect of the tower wake, even though many experiments show a correlation of the wind turbine tower wake with the characteristics of the turbine rotor wake, no convincing conclusion was ever drawn. Measurements by Maeda [6] in the wake of a single upwind three-bladed turbine in a low turbulence uniform flow ($TI \approx 1\%$) imply that the interaction between the tower and rotor wake forces the maximum velocity deficit to appear below hub height. The wake downward displacement disappeared when the incoming flow was fully turbulent ($TI \approx 15\%$), due to a reduced size of the tower cylinder wake.

Prepared using weauth.cls [Version: 2010/06/17 v1.00]

In other model scale experiments, the turbine wake structure is reported to alter its shape and position while evolving downstream from the rotor, but the presence of the tower was not considered as a possible explanation. Medici and Alfredsson [7] report a strong downward velocity component in the wake of a two-bladed model turbine ($D = 0.18\ m$) positioned in a low turbulence uniform flow. The authors suggest that the downward shift is due to an interaction with the boundary layer on the wind tunnel floor, but did not investigate the possible effect of the wind turbine tower.

In the TNO experiments [8], as analyzed by Crespo et al. [9], the wake mean line is reported to move below the turbine hub height and the wake to expand more in the vertical than in the horizontal direction, but the influence of the turbine tower was not listed as a reason.

At full-scale, Helmis et al. [10] note that the wake of the turbine tower still influences the velocity profiles at least down to $1D$ rotor diameters downstream from the turbine. The authors infer that that the presence of the tower wake affects the rotor wake evolution in a non-linear way, but did not elaborate more.

The downshift of the wake maximum velocity deficit and a different expansion rate in the vertical and horizontal direction were also observed in many of the experiments on a three bladed wind turbine operated in the wind tunnel of the NTNU University, Trondheim, as reported in [11], [12] and [13].

For this reason, a set of dedicated model scale experiments was designed, with the objective of improving the understanding of the effect of the wake tower on the symmetry of wind turbine wakes, both in single and tandem operation.

2. EXPERIMENTAL SETUP

A sketch of the experimental setup is drawn in figure 1. The turbines were designed in 2008 explicitly as test cases, which is the reason for some of the design compromises on the turbine geometry, which will be addressed in this section. See also the discussion in Krogstad and Eriksen [13] for further details.

The turbines have the same three bladed upwind rotors, but a somewhat different rotor diameter, $D_1 = 0.947\ m$ and $D_2 = 0.894\ m$, respectively, due to different hub sizes. The tests were carried out in the closed loop wind tunnel of the Department of Energy and Process Engineering, at the Norwegian University of Science and Technology of Trondheim. The inlet test section is $W = 2.71\ m$ wide, $H = 1.81\ m$ high, and $L = 12\ m$ long. This is a length which corresponds roughly to $13D$. The height of the wind tunnel was adjusted in order to have a zero pressure gradient when the empty tunnel was run at the test reference velocity, $U_{ref} = 10\ m/s$. At this speed, the flow at the inlet is characterized by a maximum measured streamwise turbulence intensity of $TI = 0.3\%$. The boundary layer thickness on the floor of the empty wind tunnel when operating at the reference velocity show that only minor interactions with the floor boundary layer is expected at the bottom part of the wake for all the analyzed downstream distances [14].

A detailed technical description of the test geometry can be found in the "Blind Test 2" paper [11], while further information about the wind tunnel geometry is reported in [15, 16, 13].

The turbines were driven through a belt transmission by a $0.37\ kW$ asynchronous motor, controlled by a Micromaster 440 Siemens inverter. In turbine T_1 the belt was fitted inside the tower, while in T_2 the belt ran behind the turbine tower. This was seen to have negligible effects on the wake development

The torque of the turbines was measured by torque sensors mounted directly on the turbine shafts, while the rotational velocity was measured via an opto-sensor which gave one pulse per rotation. The turbine thrust was measured by means of a six component aerodynamic balance positioned under the tunnel test section.

The drag of the turbine tower was measured by separate tests and subtracted from the thrust measurements, which means that the C_T values reported (see figure 2b) are relative to the rotor only.

For force, torque and rotational speed measurements of the turbines, the instruments were sampled for $60\ s$ at the rate of $30\ Hz$.

2.1. Analyzed Setups

The experiment was organized in three subsequent phases.

In the first phase of the experiment, a single turbine (T_2) was horizontally centered in the wind tunnel, at $2D$ from the inlet section, which was the minimum distance for which the inlet velocity profile was found to be independent of the operating conditions of the turbines. The rotor was rotating in counter-clockwise direction if observed from upstream. The performance of the single turbine was measured, together with the 3D wake mean velocity field in a $Y - Z$ grid at different downstream distances, $X = [0.6D, 1D, 1.5D, 2D, 3D]$ by means of a five hole pitot probe, together with the relative performance and thrust curves.

In a second step, in order to investigate the effect of the turbine tower on the wake symmetry, a second tower, manufactured in wood, was positioned above the turbine nacelle, symmetrical to the original tower, and the 5-hole pitot probe measurements were repeated at X=3D. The rationale behind this experiment was to understand the effect of tower on the flow structure.

DOI: 10.1002/we
Prepared using weauth.cls

In the last phase, the performance and the wake behind the turbine tandem running with a $3D$ downstream separation was measured.

The upstream turbine, T_1 was positioned $2D$ from the inlet to the test section, while the second turbine T_2 was positioned $S = 3D$ downstream, which allowed sufficient space for wake measurements down to $X = 4D$. The second turbine rotor was also rotating counterclockwise when observed from upstream.

2.2. Blade and airfoil

The blades used a NREL S826 airfoil section from root to tip. They are machined in aluminum, sufficiently stiff to make aeroelastic deformations negligible. The chord length at the tip is $2.58\ cm$, the total length of the blade is $0.44\ m$, and the twist varies from 38° at the root to -0.71° at the tip. The blade chord length was designed to be three times wider than what a geometrically upscaled turbine would need, in order to increase the local Reynolds number. The tip of the blade was sharply cut in order to generate strong tip vortices. A detailed description of the blade geometry can be found in [17, 13]. The rotor solidity σ, defined as the frontal area of the blades over the rotor total area, is approximately $\sigma = 9\%$.

The S826 airfoil was originally developed to be used in the tip regions of variable rotational speed rotors with highly tapered blades, see [18]. It is characterized by high lift coefficients and a separation ramp at the back which gives gentle stall characteristics, see [19]. Low Reynolds number ($Re_c < 10^5$) experiments from Sarmast [20] highlighted a hysteresis in the linear part of the lift curve ($5^\circ < \alpha < 10^\circ$), due to the onset of laminar separation bubbles. The measurements also revealed the presence of a static post-stall hysteresis at all the tested Reynolds numbers, $4 \cdot 10^4 < Re < 1.2 \cdot 10^5$.

The mean free stream velocity across the rotor area was $U_{ref} = 10.0 \pm 0.1\ m/s$ in the empty tunnel, with a maximum streamwise turbulence intensity of 0.3%.

2.3. Probes

The five hole pitot probe had an hemispherical head with a diameter of $15\ mm$, and was calibrated for a wide range of inflow angles ($\pm 20^\circ$) following the procedure indicated by Morrison et al. [21]. Further details about the calibration process and about the probe geometry can be found in [22].

The signal from the differential pressure transducers was sampled at $100\ Hz$ for a minimum time of $60\ s$.

The probes were mounted on a computer controlled three-axis traversing system which could be programmed to move and take measurements in a predefined grid of points in space.

2.4. Non-dimensional parameters

The conventional definitions for tip speed ratio, power coefficient and thrust coefficients were used, see e.g. [15], where the frontal area for each turbine was calculated using the actual rotor diameter, $D_1 = 0.947\ m$ and $D_2 = 0.894\ m$, and the reference velocity of $U_{ref} = 10\ m/s$ was used for both turbines. All dimensions were scaled by means of a nominal diameter of $D = 0.9\ m$, i.e. $x = X/D$, $y = Y/D$ and $z = Z/D$ etc. The mean velocity profiles were normalized as $u = \overline{U}/U_{ref}$ and the overbar indicates time averaging, $\overline{\square} = \langle \square \rangle$.

The tip speed ratio, (TSR or λ_i), was calculated for each turbine as $\lambda_i = \omega_i \cdot D_i/(2U_{ref})$ (no summation over i), where ω_i is the turbine rotational speed in $[rad/s]$ and D_i is the actual diameter of the turbine. Similarly, the tip Reynolds number was defined for each turbine as $Re_c = U_{tip}\ c/\nu$, where c is the local chord, ν is the air kinematic viscosity and U_{tip} is the relative velocity at the tip, i.e. $U_{tip} = \sqrt{U_{ref}^2 + (\omega_i \cdot D_i/2)^2}$ (again no summation over i).

2.5. Blockage effect

Due to blockage, the actual velocity experienced by the turbine in the test section is higher than the reference velocity, leading to an overestimation of the power and thrust coefficients. The rotor blockage ratio σ_b for the current configuration, defined as $\sigma_b = (\pi D^2)/(4W \cdot H)$ was $\sigma_b = 11.8\%$. In the first phase of the experiments, the rotational axis of the turbine was located $0.05D$ below the tunnel centreline. Hence, considering the additional presence of the turbine tower, the blockage was higher on the lower side of the test section ($\sigma_l = 18.9\%$) than on the upper side ($\sigma_u = 10.5\%$). [14] reports a thorough discussion on the blockage for the current experiments, showing that the power and thrust coefficient at the turbine optimum are only marginally affected by blockage.

The blockage exerted by the wake itself also plays an important role in the development and spreading rate of the wake, as reported by [23]. Fuglsang et al. [24] suggest that the wake blockage of a wind turbine rotor can be neglected if the wake can expand freely while evolving downstream. In the current experiment, the horizontal dimension of the wind tunnel ($\approx 3D$) is large enough to allow the free expansion of the wake at the measured downstream stations. In the vertical direction, the rotor hub height of $1D$ is acceptable and comparable to full scale situations, while the $1.3D$ distance between the hub and the tunnel roof is likely to block the expansion of the wake, as also discussed in [15]. On the grounds of the previous discussion, it was decided not to attempt any blockage correction for the data.

2.6. Scaling effects

Although the current experiments are not directly representative of a full scale case, it is important to make sure that the wake has a physically correct structure.

For a perfect scaling between model and full scale, both the tip speed ratio and the local chord Reynolds number similarity must be achieved. Although it is not difficult to match the tip speed ratio of a full scale turbine, the relatively small rotor diameter implies high rotational speeds, which might in return induce strong centrifugal and Coriolis forces and improve the post-stall performance of the airfoil, see [25].

For the upstream turbine running at optimum performance, the local Reynolds number at the blade tip was $Re_c = 10^5$, at least one order of magnitude lower than for a full scale wind turbine. Grant et al. [26] indicate that the local Reynolds similarity constraint can be relieved if the lift coefficient at the outer regions of the rotor does not significantly differ from the full scale case. If this condition is not met, differences between the model and the full scale rotor loads arise, and the lower induction at the model rotor influences the downstream convection of the wake structure. Data in [20] confirmed that the S826 airfoil lift coefficient curve for a local Reynolds number of $Re_c = 10^5$ almost overlaps the high Reynolds number experimental data in [19], which guarantees that an acceptable Reynolds scaling was achieved at least for the upstream turbine.

The local Reynolds on the downstream turbine rotor is believed to represent less of an issue, since the high turbulence flow induced by the upstream turbine is likely to suppress any low Reynolds effect and make the airfoil performance Reynolds independent.

The wake generated by the support tower should also be correctly scaled. In the current experiments, the Reynolds number based on the diameter of the downstream turbine tower and the freestream velocity was $Re^T \approx 10^5$, while in a full scale case this number can be as high as $Re^T \approx 10^7$. Under these conditions, according to the measurements in [27], the model tower drag coefficient is twice the full scale one. On top of that, the ratio between the tower and the rotor diameter at model scale is twice as big as for a typical full scale case, so we expect the velocity deficit induced by the tower to be more intense in the model tests than for a real wind turbine.

2.7. Error analysis

The experimental error on the thrust and performance measurements was calculated with a 95% confidence interval. For T_1, the uncertainty was $\pm 3\%$ on the peak efficiency and $\pm 2\%$ on the thrust coefficient at peak performance. The uncertainty on the mean velocity were also calculated with a 95% confidence interval following the method of [28]. The uncertainties were averagely below 5% of the measured value.

3. RESULTS

3.1. Characteristic Curves

In the first section we will briefly present the efficiency and cite curves for the turbines under examination. The same curves are described in detail in [13, 11], but they are reported here for the sake of completeness.

In figure 2a the black dots represent the power coefficient of the upstream turbine. At low tip speed ratios, $\lambda_1 < 3$, the rotor is fully stalled and the power production is low. At $\lambda_1 = 4$, the flow reattaches in the inner part of the rotor, and the performance increases until its maximum $C_P = 0.468$ for $\lambda_1 = 6$. For higher tip speed ratios, the angle of attack across the rotor decreases rapidly. The lift produced in the outer section of the blade decreases, while the inner sections of the rotor produce negative lift and begin to work in a propeller state, feeding energy into the flow. When these two counteracting forces even out, the rotor reaches the runaway point, $\lambda_1 = 11.5$.

The cite curve, in figure 2b, is overall quite regular. At around $\lambda_1 = 4$, where the flow from deeply stalled becomes attached and a large amount of lift is generated, the cite has a steep increase. As we approach the runaway TSR, the cite increases less dramatically due to the inner sections of the rotor working as propellers, generating negative lift.

Despite its regular overall shape, the performance curve showed a dip at $\lambda_1 = 5.5$, outside of the tip speed ratio range where stall is expected, probably due to a minor laminar separation.

The performance and cite coefficients of the turbine equipped with the double tower configuration was also measured, but the deviations from the single tower case were within experimental uncertainty, therefore the values were not included.

The maximum efficiency of T_2 when operating in the wake was $C_P = 0.128$, which corresponds to 28.5% of its maximum efficiency in free flow, see [13]. Despite the low local Reynolds number on the downstream rotor, the power coefficient curve in figure 2a was smooth and did not show any dip. This suggests that the turbulence generated in the wake of the upstream turbine suppresses the laminar separation on the downstream turbine rotor.

Figure 2b displays the cite coefficient for the two turbines. At runaway conditions, $\lambda_1 = 11.5$, the upstream turbine cite coefficient was $C_T = 1.2$, close to the value for a solid disk. At optimum performance, $\lambda_1 = 6$, the coefficient was

Wind Energ. 0000; **00**:1–16 © 0000 John Wiley & Sons, Ltd.
DOI: 10.1002/we
Prepared using weauth.cls

$C_T = 0.86$, while at lower tip speed ratios ($\lambda_1 < 4$) the flow on the inner section was stalled and led to a sudden drop on the cite. At $\lambda_1 > 7$ the cite increased smoothly due to the gradual increasing negative contribution on the total cite from the inner sections of the rotor feeding energy back into the flow.

Figure 2b also shows that the cite distribution for T_2 has none of the irregularities found for T_1. When operating alone, T_2 had its peak power coefficient at $\lambda_2 \approx 6$. This is shifted down to $\lambda_2 \approx 4$ when it operates in the wake of T_1, suggesting that the effective velocity across the rotor plane has dropped from $U_{ref} = 10m/s$ to about $6.5m/s$.

3.2. Wake measurements in a cross sectional plane, single turbine ($\lambda_1 = 6$)

By a quick comparison between figure 3a and 3a, it is clear that the wake changes drastically while evolving downstream from the rotor disc. At $X = 0.6D$, the velocity deficit across the rotor disk was almost uniform, with a mean value of $U/U_\infty = 0.5$. On the other hand, close to the blade root, where the blade extracts the energy less efficiently and part of the flow bypasses the rotor, the streamwise velocity had a relative maximum, $U/U_\infty = 0.6$.

In the lower half of the rotor disc, the flow velocity was averagely higher than in the upper half, meaning less energy is extracted by the rotor disc. This may be explained by the fact that, in turbine T_1, the tower is quite close ($0.1D$) to the rotor plane, see figure 1. The tower induces a decrease in the fluid speed, and modifies the angle of attack on the rotor, which in turn decreases the airfoil efficiency.

The wake of the tower was easily recognizable as a low velocity area right behind the cylinder. The wake was bent on the left, due to the uneven advection by the rotation of the wake. The magnitude of the tangential component of the spanwise velocity vector is represented as a contour plot in figure 4a, to which the vector plot is superimposed.

The tangential component of the spanwise velocity field was calculated with respect to the wake vortex center, which was visually individuated and marked with the $\otimes$ symbol on the velocity plots. As we can see in figure 4a, at $X = 0.6D$ the wake vortex center lays on the turbine rotational axis. The tangential velocity is highest close to the turbine axis, and lowest at the rotor rim, therefore the tower wake is advected further at the center of the wake, see also figure 3a. The tangential velocity is also close to zero in the tower wake area, where the flow is disturbed by the presence of the tower. The radial velocity, in figure 5a, was almost univocally null, indicating that the flow was practically only tangential. In the lower part of the turbine rotor wake, momentum is entrained from the rotor disc into the tower wake, since the radial velocity is slightly negative.

At $X = 1D$, in figure 3b, the tower wake was still deep and well defined, and continued to rotate clockwise, dragged by the rotor wake. On the other side of the turbine axis, the high velocity area generated by the flow bypassing the rotor also rotated in clockwise direction.

The overall rotor wake had a regular circular shape, with sharp gradients separating the wake from the free flow, showing very small amounts of turbulent diffusion. This indicates that the wake helical vortex structure is stable, as it is expected for a turbine working at optimum and in a low turbulence incoming flow.

Nevertheless, the whole wake structure had a tendency to move toward the wind tunnel floor: the center of rotation of the mean wake vortex was in fact located $0.1D$ below the rotor centerline.

Further downstream, at $X = 1.5D$, in figure 3c, the overall rotor wake shape started to lose the circular shape, as a probable consequence of the destabilization of the vortex system. The wake was $0.1D$ wider than high, and the center of rotation was located well below the turbine rotational axis. The tower wake was still visible as a low velocity area on the left part of the rotor disc. The high velocity area also rotated further, appearing as relative velocity peak ($U/U_\infty = 0.6$) below the turbine rotational axis.

At $X = 2D$, in figure 3d, the footprint of the tower wake inside the rotor disc was almost entirely eroded by turbulent diffusion, while the high velocity fluid was still located below the turbine rotational axis. Except for these two contributions, the velocity profile inside the rotor disc was quite smooth, with an average value of $U/U_\infty = 0.5$. The gradients at the rotor rim were smoother than at the previous downstream distances, due to turbulent diffusion pumping fresh momentum inside the wake. The overall shape of the rotor wake was not axisymmetric, indicating a higher expansion of the wake in the horizontal than in the vertical direction.

At $X = 3D$, in figure 3e, the velocity deficit inside the rotor disc was quite homogeneous. Momentum flowed into the wake, due to cross-stream turbulent transport, and the average mean velocity was higher than at the previous downstream distances (see fig 3c), as expected.

At this point, the wake had two main distinctive differences with respect to the near wake measured at $X = 0.6D$: first, the wake vortex center appeared to be below the wake centerline, on the left half of the wind tunnel, right besides the higher velocity zone. This is even clearer in figure 4b, where the wake vortex center is marked by the $\otimes$ symbol. Secondly, the wake was not circular, larger in the horizontal than in the vertical dimension.

Figure 5b suggests that both effects can be tracked back to an uneven momentum entrainment from the free flow into the rotor wake. Most of the free-stream momentum is entrained into the wake in the top-tip region rather than in the side region of the turbine wake, as marked by a strong negative radial velocity component. On the other hand, the momentum

which replenished the the tower wake velocity deficit comes from inside the turbine rotor disc, as demonstrated by the positive radial velocity right below the turbine hub.

This uneven momentum entrainment, induced by the presence of the turbine tower, pushes the wake structure downward. In order to further demonstrate this, a dedicated experiment was designed.

3.3. Wake measurements in a cross sectional plane, single turbine with an additional tower ($\lambda_1 = 6$)

A tower with the same geometry of the original one was manufactured and mounted vertically up on top of the nacelle of turbine T_2, in order to re-establish the geometrical symmetry of the test case. The turbine was positioned at $2D$ from the wind tunnel inlet section. The wake of the turbine, running at $\lambda_2 = 6$, was traversed on a yz plane at $X = 3D$ by means of a 5-hole pitot probe in a uniform, low turbulence flow, with $U_\infty = 10\ m/s$.

Figure 6a shows that using a symmetric geometry produced a symmetric and regular wake. The wake vortex was centred at the turbine axis, and the spanwise velocity field was symmetric both with respect to $y = 0$ and $z = 0$.

The analysis of the tangential component of the spanwise velocity, in figure 7a, confirms that the vortex downstream of the turbine is actually symmetrical. Two zones of high tangential velocity appear at -45° and 135° azimuthal position. In the base case, figure 4b, only one zone of high tangential velocity was observed, at -75° azimuthal position. The radial velocity plot shows that the momentum is flowing from the turbine wake into the tower wake, while fresh momentum from the free flow is entrained on the sides, rather than on the top tip region, as in figure 5b. This is the reason why no downshift of the wake was observed in the wake of the turbine with the double tower configuration.

3.4. Wake measurements in a cross sectional plane, two turbines ($\lambda_1 = 6$,$\lambda_2 = 4$)

In the light of the previous elements, the wake behind a cluster of two turbines will be analyzed.

Figure 8a shows the contour plot of the non-dimensional streamwise velocity at $X = 0.6D$ downstream from the turbine tandem, running at $\lambda_1 = 6$ and $\lambda_2 = 4$. The downstream turbine was immersed in the wake of the upstream turbine, which had developed for three rotor diameters. The inflow on the second turbine, corresponding to the flow measured in figure 3e plus the induction generated by the second turbine, was quite non-homogeneous and was characterized by a low average velocity.

As a general remark, we can see that the velocity in the turbine tandem wake was lower than in the single turbine in figure 3a, since more momentum was extracted by the two turbines overall. On the other hand, the mean velocity gradient between the tandem wake and the free flow were less steep, and it was not possible to distinguish the point where the downstream turbine wake merged with the upstream turbine one.

The wake was wider in the spanwise z than in the wall normal y direction, as in the single turbine case. The centre of the wake vortex was located below hub height, at $(-0.025D, -0.1D)$, suggesting an overall downward movement of the wake structure already at $X = 0.6D$. This is in contrast with the observations in the near wake of a single turbine, figure 3a, where the wake vortex was centered at the turbine axis.

The streamwise velocity was not homogeneous across the rotor disc, but was on average lower in the upper half of the rotor disc ($U/U_\infty \approx 0.3$) than in the lower part ($U/U_\infty > 0.4$), as also remarked for the single turbine case, see figure 3a. This may be tracked back to the influence of the turbine tower, which changes the inflow conditions on the lower half of the turbine rotor and reduces the efficiency of the energy extraction. Inside the rotor disc, the turbine tower wake was not clearly discernible from the rotor wake, except for a low velocity spot at the intersection between the tower and the rotor rim. Due to turbulent diffusion, momentum was more effectively transferred inside the tower wake, resulting into a nearly null effect if the tower wake on the overall flow pattern.

Due to the uneven momentum extraction across the rotor disc, a high velocity zone appeared behind the rotor hub, as it was also observed for the single turbine wake.

At $X = 3D$, in figure 8b, the wake was shaped as an irregular oval, approximately 10% wider in the z direction than in the y direction. The tower wake was not distinguishable as a separate wake, but was totally merged into the turbine rotor wake. In fact, the overall mean velocity profile had only one, well-defined, minimum, $U/U_\infty = 0.31$, located at (0.1D,-0.2D), contrarily to the single turbine case, see figure 3e. This is also a consequence of the higher turbulent transport in the wake, consequence of the averagely higher turbulent stress levels that can be experienced behind a turbine cluster (see also [11, fig. 6]).

Other interesting details on the wake evolution arise by the analysis of the spanwise velocity field. At $X = 0.6D$, in figure 9a, the tangential velocity on the right half of the wake was three times as on the left half, as already noted in figure 4a for the single turbine wake, but the tangential velocity was averagely higher than for the single turbine case. In fact, the wake rotation generated by the second turbine was superimposed to the rotation of the wake of the wind turbine, and the effect of the tower wake was less intense, due to the increased turbulence levels in the turbine wake. In the single turbine case, the tangential velocity magnitude was univocally zero outside of the rotor disc. In the turbine tandem case, the tangential velocity is significantly different from zero outside of the rotor rim, especially on the left half plane. The

Wind Energ. 0000; **00**:1–16 © 0000 John Wiley & Sons, Ltd.
DOI: 10.1002/we
Prepared using weauth.cls

rotation in this portion of fluid is likely to be a legacy of the upstream turbine wake, which moved towards the left side of the fluid domain while evolving downstream, as discussed in section 3.2.

Figure 9b shows that the tangential velocity maximum at $X = 3D$ was positioned on the positive z half-plane, but its absolute value was 30% lower than at $X = 0.6D$, and located $0.05D$ further from the vortex centre. In fact, as the mean velocity in the turbine wake decreases, the radius of the streamwise vortex increases as a consequence of vorticity transport in the fluid, and the tangential velocity peak moves towards larger radial positions.

Despite the above mentioned differences, the wake vortex center in the double turbine case was in the same position as for the single turbine case. This suggests that, both in free stream and wake operation, the effect of the tower on the wake symmetry is very similar.

On the other hand, figure 10a shows the presence of a strong fresh fluid entrainment in the top tip region of the tandem wake already at $X = 0.6D$, contrarily what was observed in figure 5a for the single turbine case. It is likely that the turbulence in the upstream turbine wake destabilizes the downstream helical vortex structure at short downstream distances, leading to an early breakdown and resulting into additional random turbulence. This process increases the turbulent transport of fresh fluid into the wake, and speeds up the wake recovery with respect to the single turbine wake.

Everywhere else the radial velocity was slightly positive, with a maximum normalized value of $v_r = 0.06$, indicating a general tendency of the wake to grow in size, especially on the sides of the rotor disc, which is a probable explanation for the wake's irregular oval shape.

At $X = 3D$ (figure 10b) the negative radial velocity zone in the upper half of the wake was wider and more intense, meaning the entrainment becomes stronger as the wake evolves downstream. In the lower part, the radial velocity was close to zero, marking an almost zero expansion in the vertical direction.

4. CONCLUDING REMARKS

In this paper the effect of the turbine tower on the symmetry of the wake flow was observed experimentally in the wind tunnel.

Measurements in the wake of a single turbine showed that the turbine tower wake generated an uneven velocity deficit inside of the rotor disc. The tower wake appeared as a distinct low velocity fluid zone, while the fluid flowing through the rotor center appeared as a high velocity zone, due to the low axial induction. This flow pattern was entrained in the turbine wake and rotated with it, persisting down to $X = 3D$ downstream, due to a relatively low mixing in the turbine wake. The analysis of the radial velocity plot showed that a net unbalance in the vertical momentum transport was generated by the presence of the turbine tower wake. As a consequence, the mean wake structure tended to shift below hub height and to grow more in the horizontal than in the vertical direction.

The correlation between the presence of the tower and the downshift in the turbine wake structure was confirmed by a dedicated experiment, where a secondary tower was mounted symmetrically on top of the turbine nacelle. The presence of the second tower wake evened out the momentum entrainment in the top and bottom tip region. Therefore, the wake vortex behind this modified test case was actually symmetrical and did not move below hub height while evolving downstream.

When the two turbines are arranged in a tandem, the wake of the first turbine becomes the inflow for the second turbine. The tandem wake shared many similarities with the wake of the single turbine, namely the downshift of the mean wake vortex and a tendency to grow more in the horizontally than in the vertical direction. Also the spanwise velocity field was qualitatively similar to the one of a single turbine, especially the strong entrainment in the top tip region. On the other hand, due to a higher mean turbulence level, a stronger fresh momentum entrainment was generated and the wake recovered faster. As a consequence, the footprint of the tower wake had a tendency to disappear more quickly, and, already at $X = 3D$ downstream from the second turbine, the wake assumed a regular streamwise velocity profile with a single well-defined minimum.

5. ACKNOWLEDGEMENTS

The authors acknowledge NOWITECH for the financial support received throughout the project. The authors also acknowledge Hedda P. Blomhoff and Heiner Schümann for their precious help in performing the experiments.

REFERENCES

1. Wilson RE. Wind-turbine aerodynamics. *Journal of Wind Engineering and Industrial Aerodynamics* 1980; **5**(3-4):357–372.
2. Okulov V, Sørensen JN. Stability of helical tip vortices in a rotor far wake. *Journal of Fluid Mechanics* 2007; **576**:1.

3. Vermeer LJ, Sørensen JN, Crespo A. Wind turbine wake aerodynamics. *Progress in aerospace sciences* 2003; **39**(6-7):467–510.
4. Chamorro F LP Porté-Agel. Flow characterization of wind-turbine wake (s) developed in a boundary layer flow with different thermal stratifications: A wind-tunnel study. *The Fifth International Symposium on Computational Wind Engineering CWE 2010*, 2010.
5. Chamorro L, Porté-Agel F. A wind-tunnel investigation of wind-turbine wakes: Boundary-layer turbulence effects. *Boundary-Layer Meteorology* 2009; **132**(1):129–149.
6. Maeda T, Yokota T, Shimizu Y, Adachi K. Wind tunnel study of the interaction between two horizontal axis wind turbines. *Wind Engineering* 2004; **28**(2):197–212.
7. Medici D, Alfredsson P. Measurements on a wind turbine wake: 3d effects and bluff body vortex shedding. *Wind Energy* 2006; **9**(3):219–236.
8. Luken E, Talmon A, Vermeulen P. Evaluation of two mathematical wind turbine wake models in various types of flows. *TNO Division of Technology for Society, Report* 1986; :86–07.
9. Crespo A, Hernández J, Fraga E, Andreu C. Experimental validation of the upm computer code to calculate wind turbine wakes and comparison with other models. *Journal of Wind Engineering and Industrial Aerodynamics* 1988; **27**(1-3):77–88.
10. Helmis CG, Papadopoulos KH, Asimakopoulos DN, Papageorgas PG, Soilemes AT. An experimental study of the near-wake structure of a wind turbine operating over complex terrain. *Solar energy* 1995; **54**(6):413–428.
11. Pierella F, Krogstad PÅ, Sætran L. Blind test 2 calculations for two in-line model wind turbines where the downstream turbine operates at various rotational speeds. *Renewable Energy* 2014; **70**:62–77.
12. Bartl J, Pierella F, Sætran L. Wake measurements behind an array of two model wind turbines. *Energy Procedia* 2012; **24**:305–312.
13. Krogstad PÅ, Eriksen PE. "blind test" calculations of the performance and wake development for a model wind turbine. *Renewable Energy* 2013; **50**(0):325 – 333, doi:10.1016/j.renene.2012.06.044. URL `http://www.sciencedirect.com/science/article/pii/S0960148112003953`.
14. Pierella F. Experimental investigation of wind turbine wakes and their interaction. PhD Thesis, NTNU 2014.
15. Adaramola MS, Krogstad PÅ. Experimental investigation of wake effects on wind turbine performance. *Renewable Energy* 2011; **36**(8):2078–2086.
16. Krogstad PÅ, Adaramola MS. Performance and near wake measurements of a model horizontal axis wind turbine. *Wind Energy* 2012; **15**(5):743–756, doi:10.1002/we.502. URL `http://dx.doi.org/10.1002/we.502`.
17. Krogstad PÅ, Lund JA. An experimental and numerical study of the performance of a model turbine. *Wind Energy* 2011; **15**:443–457.
18. Tangler JL, Somers DM. Nrel airfoil families for hawts. *Proceedings of the American Wind Energy Association Windpower Conference, Washington*, National Renewable Energy Laboratory, 1995.
19. Somers D. Design and experimental results for the s825 airfoil. *Technical Report NREL/SR-500-36344*, National Renewable Energy Laboratory 1999.
20. Sarmast S. Numerical study on instability and interaction of wind turbine wakes. PhD Thesis, KTH Stockholm 2013.
21. Morrison G, Schobeiri M, Pappu K. Five-hole pressure probe analysis technique. *Flow Measurement and Instrumentation* 1998; **9**(3):153 – 158, doi:10.1016/S0955-5986(98)00023-5. URL `http://www.sciencedirect.com/science/article/pii/S0955598698000235`.
22. Schümann H. The interactions between wind turbines caused by their respective wakes. Master's Thesis, NTNU 2012.
23. Barlow J, Rae W, Pope A. *Low-speed wind tunnel testing*, *Recherche*, vol. 67. 3 edn., Wiley-Interscience, 1999.
24. Fuglsang P, Bak C, Gaunaa M, Antoniou I. Design and verification of the risø-b1 airfoil family for wind turbines. *Journal of Solar Energy Engineering* 2004; **126**:1002.
25. Hansen M. *Aerodynamics of wind turbines*. 2nd edn., Earthscan, 2008.
26. Grant I, Parkin P, Wang X. Optical vortex tracking studies of a horizontal axis wind turbine in yaw using laser-sheet flow visualisation. *Experiments in Fluids* 1997; **23**(6):513–519.
27. Delany N, Sørensen N. Low-speed drag of cylinders of various shapes. *Technical Report 3038*, National Advisory Committee for Aeronautics 1953.
28. Benedict LH, Gould RD. Towards better uncertainty estimates for turbulence statistics. *Experiments in Fluids* 1996; **22**(2):129–136, doi:10.1007/s003480050030. URL `http://dx.doi.org/10.1007/s003480050030`.

LIST OF FIGURES

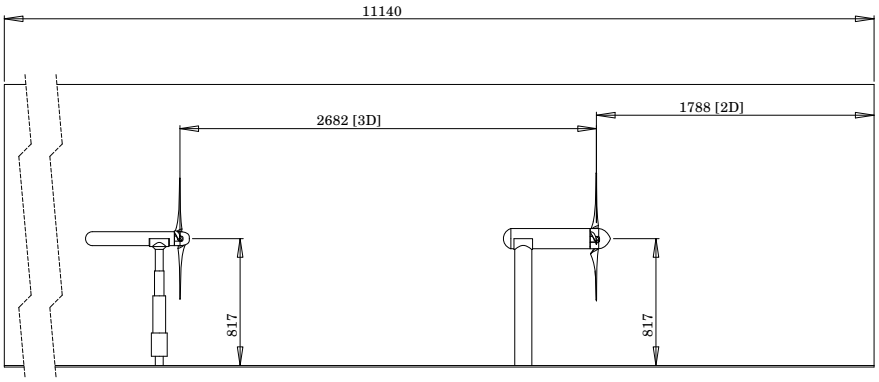

Figure 1. Experimental setup, side view. The flow is from right to left.

Wind Energ. 0000; **00**:1–16 © 0000 John Wiley & Sons, Ltd.
DOI: 10.1002/we
Prepared using weauth.cls

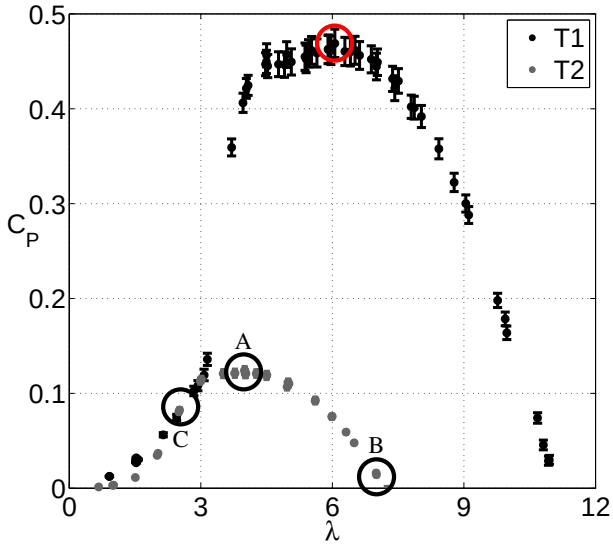

(a) Power Coefficient

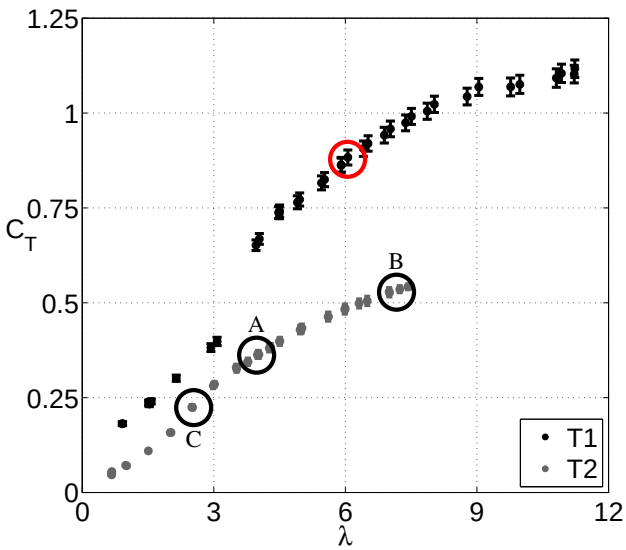

(b) Thrust Coefficient

Figure 2. Characteristic curves. Black: T_1, Grey: T_2. The measurements on T_2 were made for T_1 running at $\lambda_1 = 6$ (red circle). **A**: $\lambda_1 = 6, \lambda_2 = 4$. **B**: $\lambda_1 = 6, \lambda_2 = 7$. **C**: $\lambda_1 = 6, \lambda_2 = 2.5$

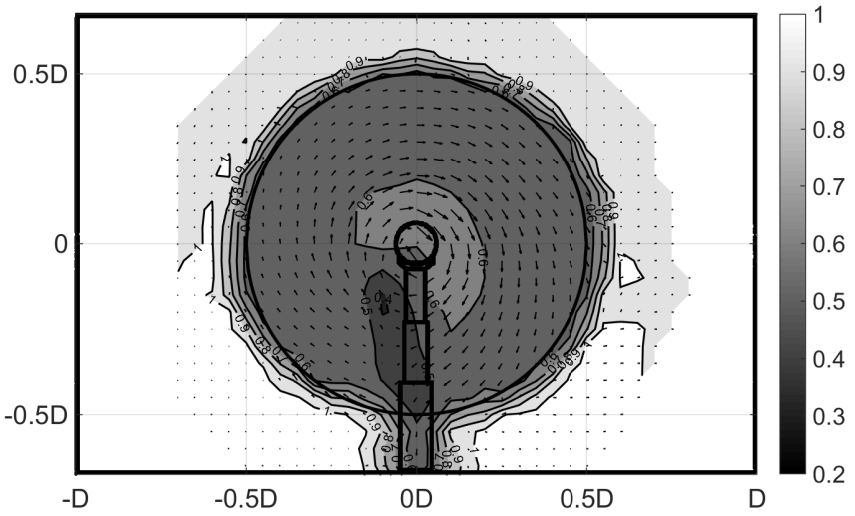

(a) U/U_∞,$X = 0.6D$

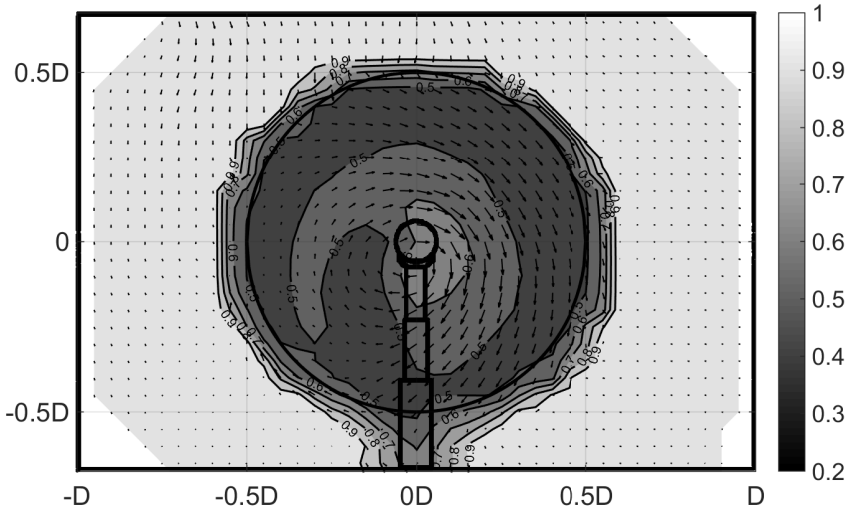

(b) U/U_∞,$X = 1D$

Wind Energ. 0000; **00**:1–16 © 0000 John Wiley & Sons, Ltd.
DOI: 10.1002/we
Prepared using weauth.cls

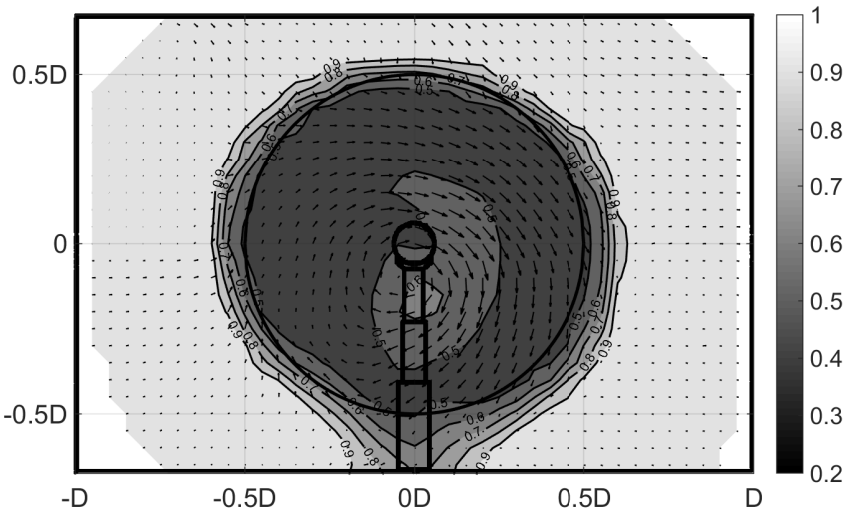

(c) U/U_∞,$X = 1.5D$

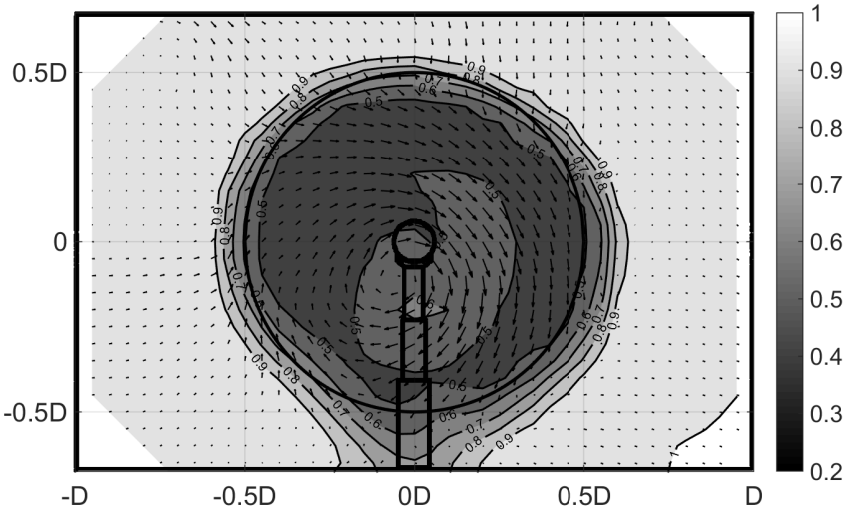

(d) U/U_∞,$X = 2D$

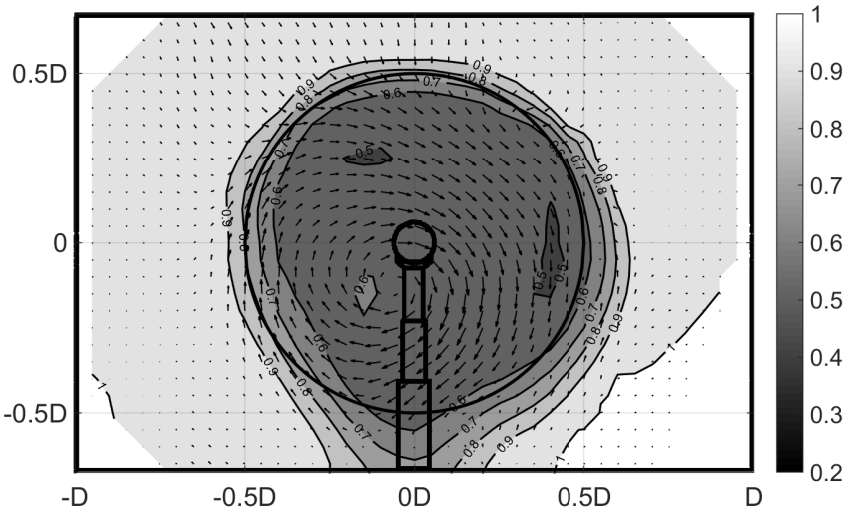

(e) U/U_∞,$X = 3D$

Figure 3. Contour plot: mean non-dimensional velocity U/U_∞ of the velocity deficit $X = 3D$ downstream from a single turbine working at $\lambda = 6$ in a low turbulence (TI=0.3%), uniform flow with $U_\infty = 10\ m/s$. It is possible to track and follow the evolution of the velocity deficit induced by the tower. Arrows: spanwise velocity field.

Wind Energ. 0000; **00**:1–16 © 0000 John Wiley & Sons, Ltd.
DOI: 10.1002/we
Prepared using weauth.cls

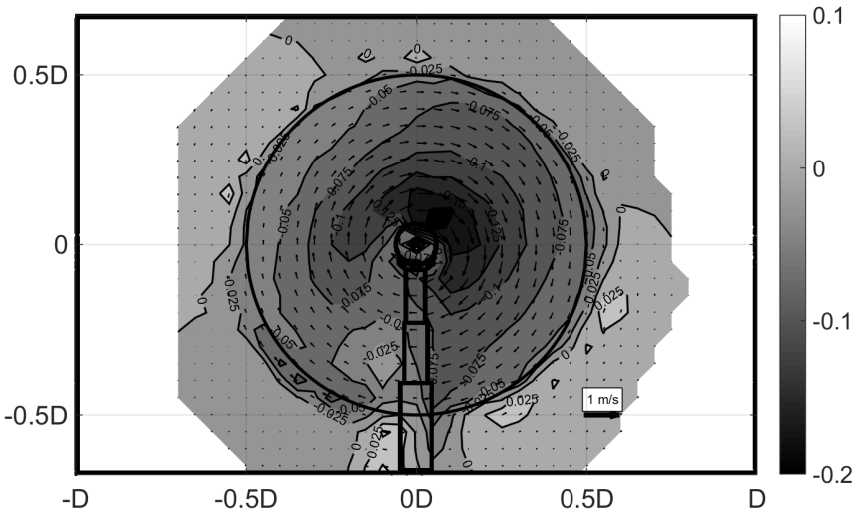

(a) $X = 0.6D$

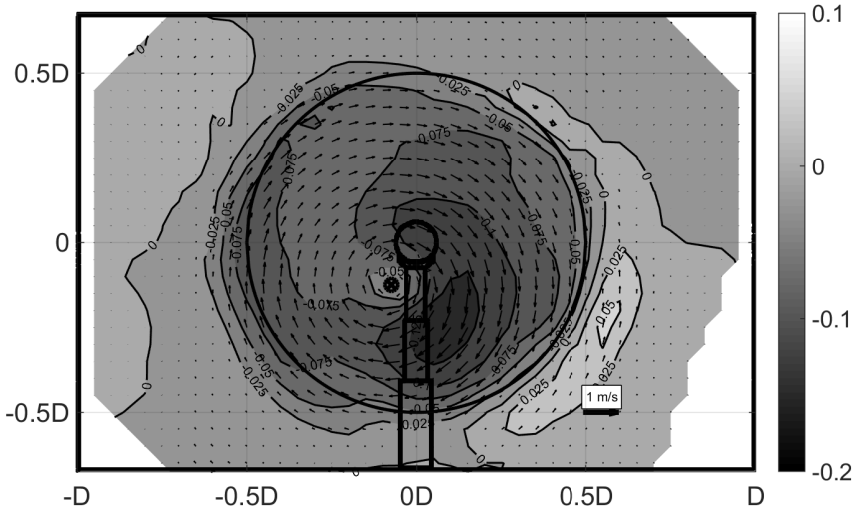

(b) $X = 3D$

Figure 4. Single turbine $\lambda_1 = 6$. Contour plot: mean tangential velocity on a spanwise plane, $\overline{V_\theta}/U_{ref}$, calculated with respect to the wake vortex centre, marked with $\otimes$. Arrows: tangential velocity field, note the reference vector.

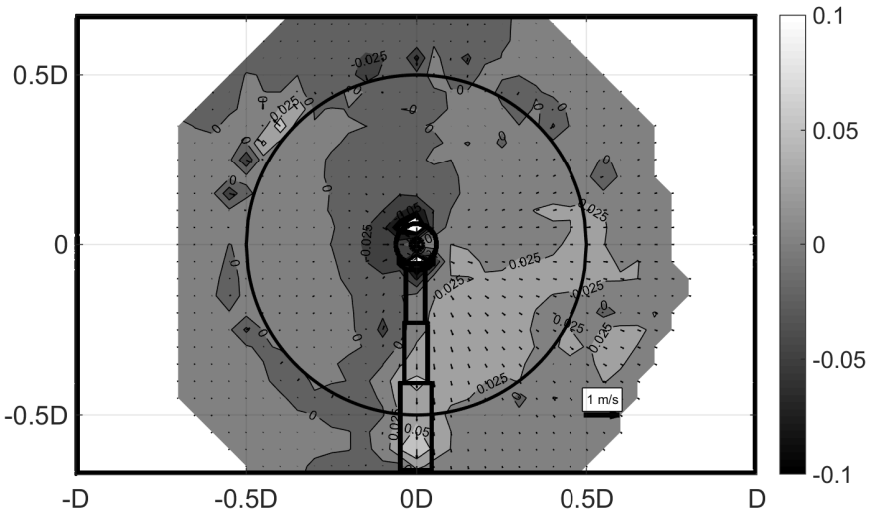

(a) $X = 0.6D$

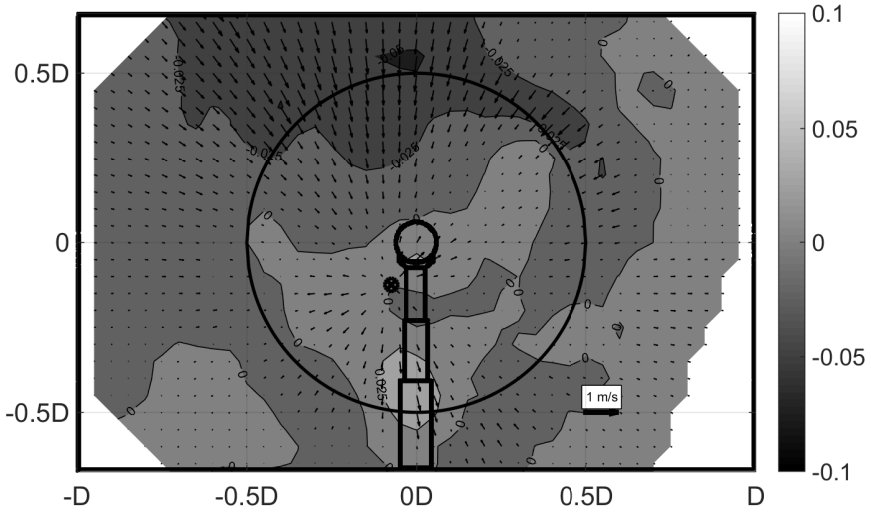

(b) $X = 3D$

Figure 5. Single turbine $\lambda_1 = 6$. Contour plot: mean radial velocity on a spanwise plane, $\overline{V_r}/U_{ref}$, calculated with respect to the wake vortex centre, marked with $\otimes$. Arrows: radial velocity field, note the reference vector.

Wind Energ. 0000; **00**:1–16 © 0000 John Wiley & Sons, Ltd.
DOI: 10.1002/we
Prepared using weauth.cls

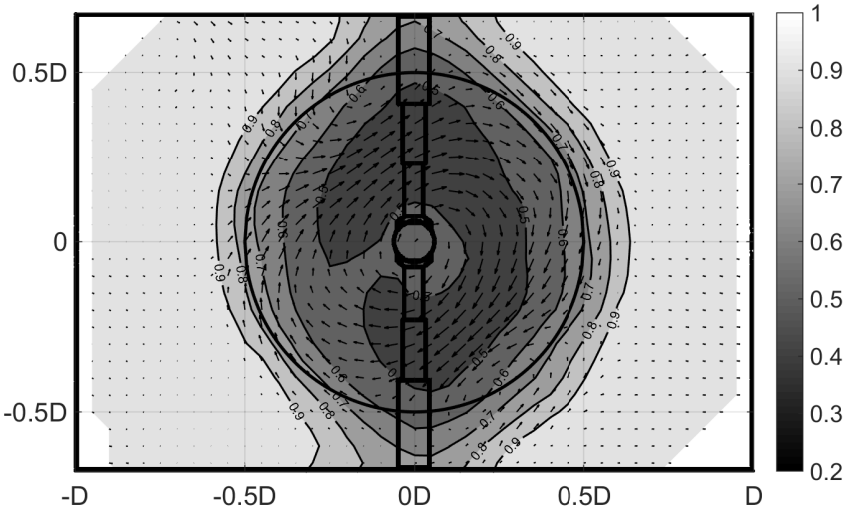

(a) Two towers, $X = 3D$

Figure 6. Only turbine T_2, ($\lambda_2 = 6$). Contour plot: mean streamwise velocity on a spanwise plane, $\overline{U}/U_{ref}$. Arrows: spanwise velocity field, note the reference vector. The mean velocity profile behind the configuration with a symmetric tower is symmetrical with respect to the $y = 0$ and $z = 0$ plane.

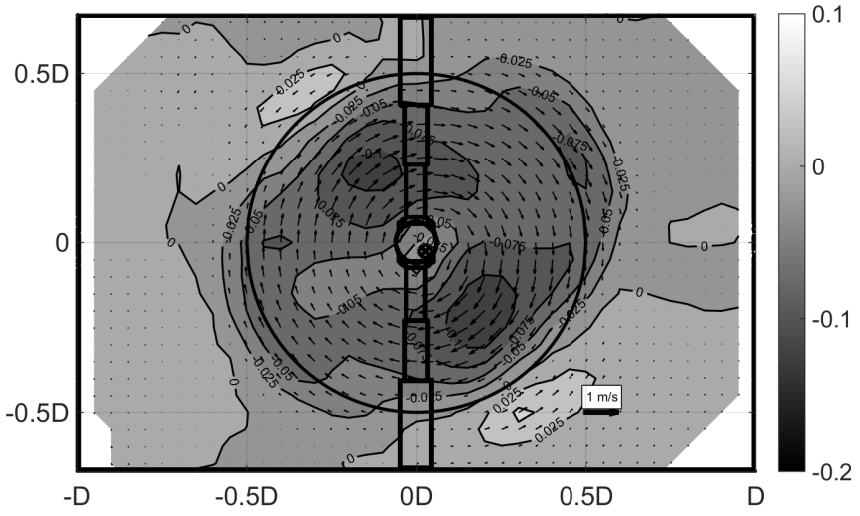

(a) Tangential velocity contour plot, $X = 3D$

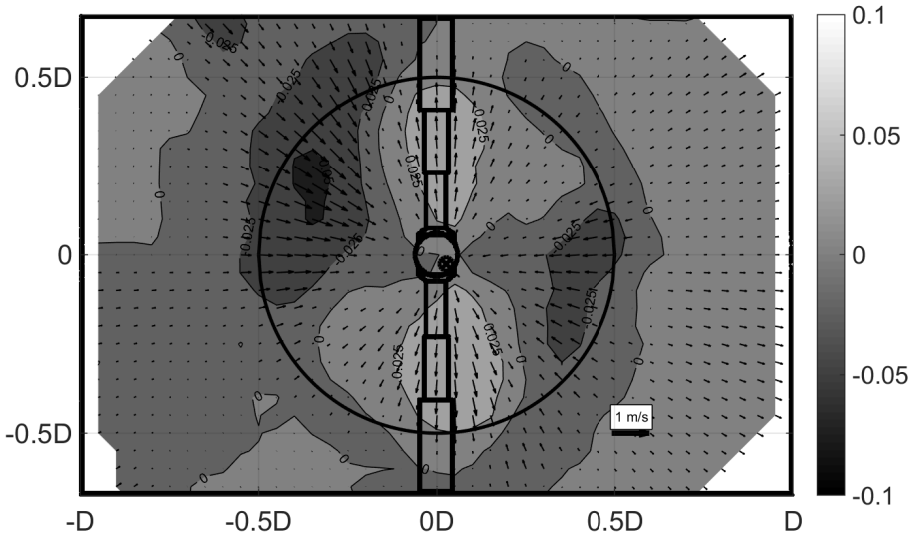

(b) Radial velocity contour plot, $X = 3D$

Figure 7. Only turbine T_2, with additional tower ($\lambda_2 = 6$). Contour plot: mean streamwise velocity on a spanwise plane, $\overline{U}/U_{ref}$. Arrows: radial and tangential velocity field, note the reference vector. The mean velocity profile behind the configuration with a symmetric tower is symmetrical with respect to the $y = 0$ and $z = 0$ plane.

Wind Energ. 0000; **00**:1–16 © 0000 John Wiley & Sons, Ltd.
DOI: 10.1002/we
Prepared using weauth.cls

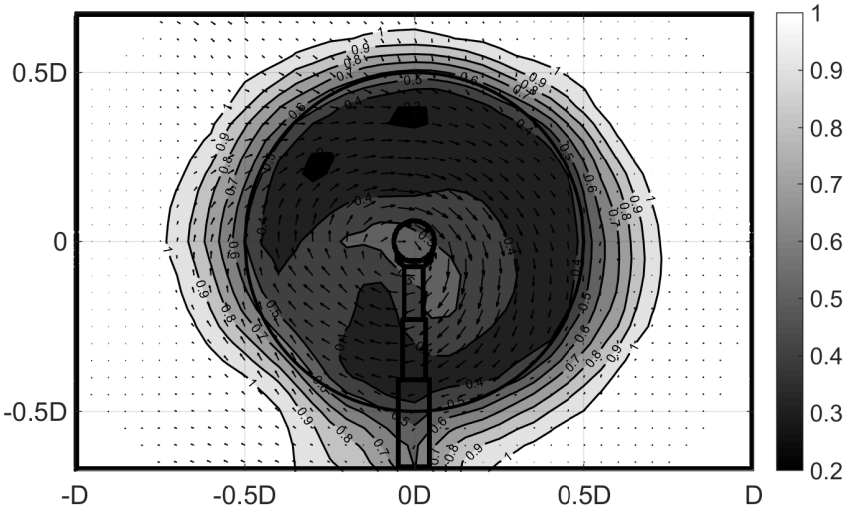

(a) $X = 0.6D$

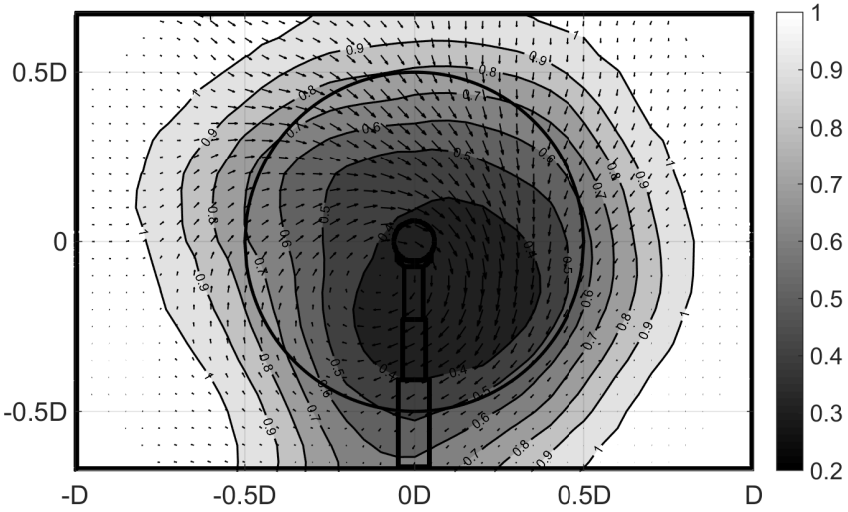

(b) $X = 3D$

Figure 8. Two turbines, downstream separation $S = 3D$, Setup A ($\lambda_1 = 6$,$\lambda_2 = 4$). Contour plot: mean streamwise velocity on a spanwise plane, $\overline{U}/U_{ref}$. Arrows: spanwise velocity field, note the reference vector.

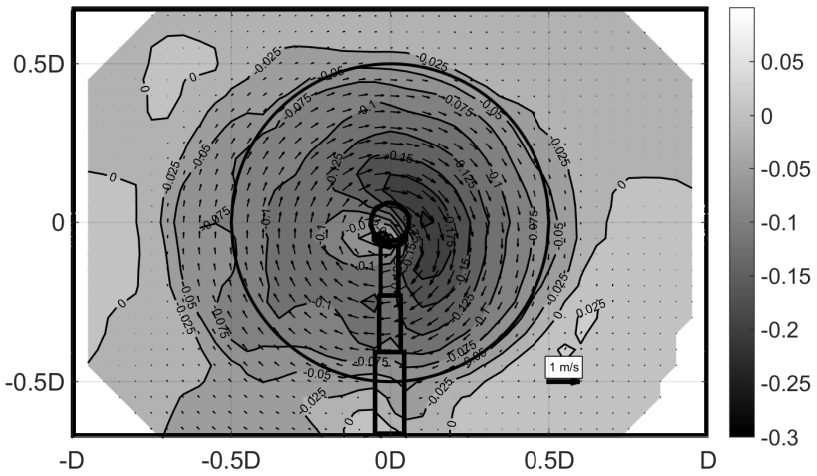

(a) $X = 0.6D$

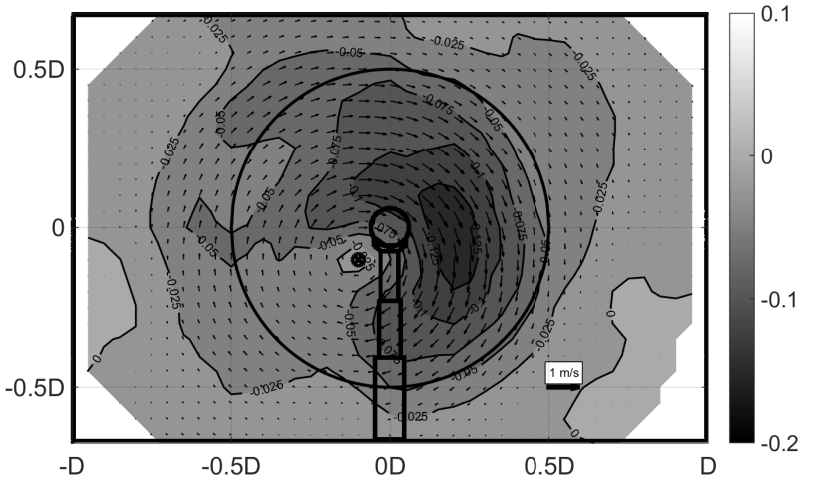

(b) $X = 3D$

Figure 9. Two turbines, downstream separation $S = 3D$, Setup A ($\lambda_1 = 6$,$\lambda_2 = 4$). Contour plot: mean tangential velocity on a spanwise plane, $\overline{V_\theta}/U_{ref}$, calculated with respect to the wake vortex centre, marked with $\otimes$. Arrows: radial and tangential velocity field, note the reference vector.

Wind Energ. 0000; **00**:1–16 © 0000 John Wiley & Sons, Ltd.
DOI: 10.1002/we
Prepared using weauth.cls

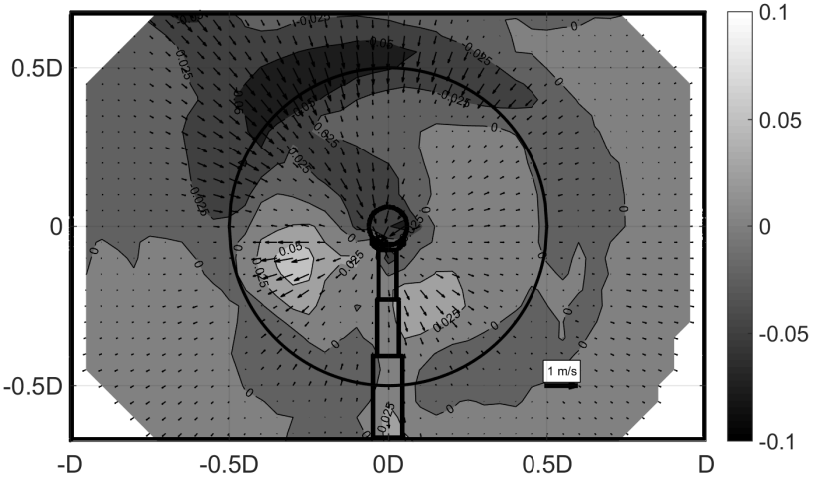

(a) $X = 0.6D$

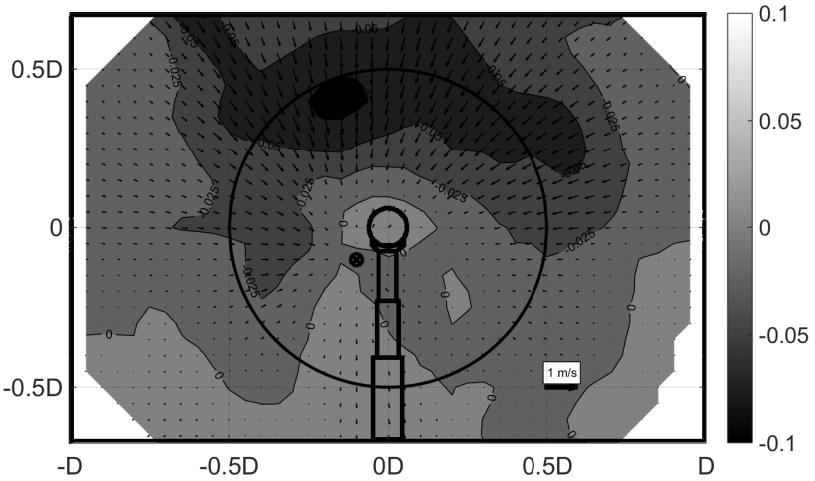

(b) $X = 3D$

Figure 10. Two turbines, downstream separation $S = 3D$, Setup A ($\lambda_1 = 6$,$\lambda_2 = 4$). Contour plot: mean radial velocity on a spanwise plane, $\overline{V_r}/U_{ref}$, calculated with respect to the wake vortex centre, marked with $\otimes$. Arrows: radial velocity field, note the reference vector.